

J. H. Klenzing, G. D. Earle, R. A. Heelis, W. R. Coley  
William B. Hanson Center for Space Sciences, The University of Texas at Dallas

## Introduction

The use of biased grids as energy filters for charged particles has been a common practice in satellite-borne instruments such as the retarding potential analyzer (RPA). It has been shown previously that the use of biased grids in such instruments creates a non-uniform potential in the grid plane, which leads to errors in inferred geophysical parameters including velocity, temperature, and composition. A simulation of ion interactions with a number of configurations of biased grids has been developed using a commercial finite-element analysis software package. Using a statistical approach, the simulation calculates collected flux from Maxwellian ion distributions with 3D drift relative to the instrument. Perturbations in the performance of flight instrumentation relative to expectations from the idealized RPA flux equation are discussed. Both single-grid and double-grid systems are modeled to investigate design considerations. Relative errors in the inferred parameters are characterized as functions of temperature and drift velocity.

## The RPA as an Energy Filter

Figure 1 shows a series of sample Maxwellian ion populations and the corresponding IV curves collected by an idealized RPA. The RPA functions by successively retarding ions below a specific energy. This allows us to relate a collected current-voltage (IV) curve to a flux density distribution.

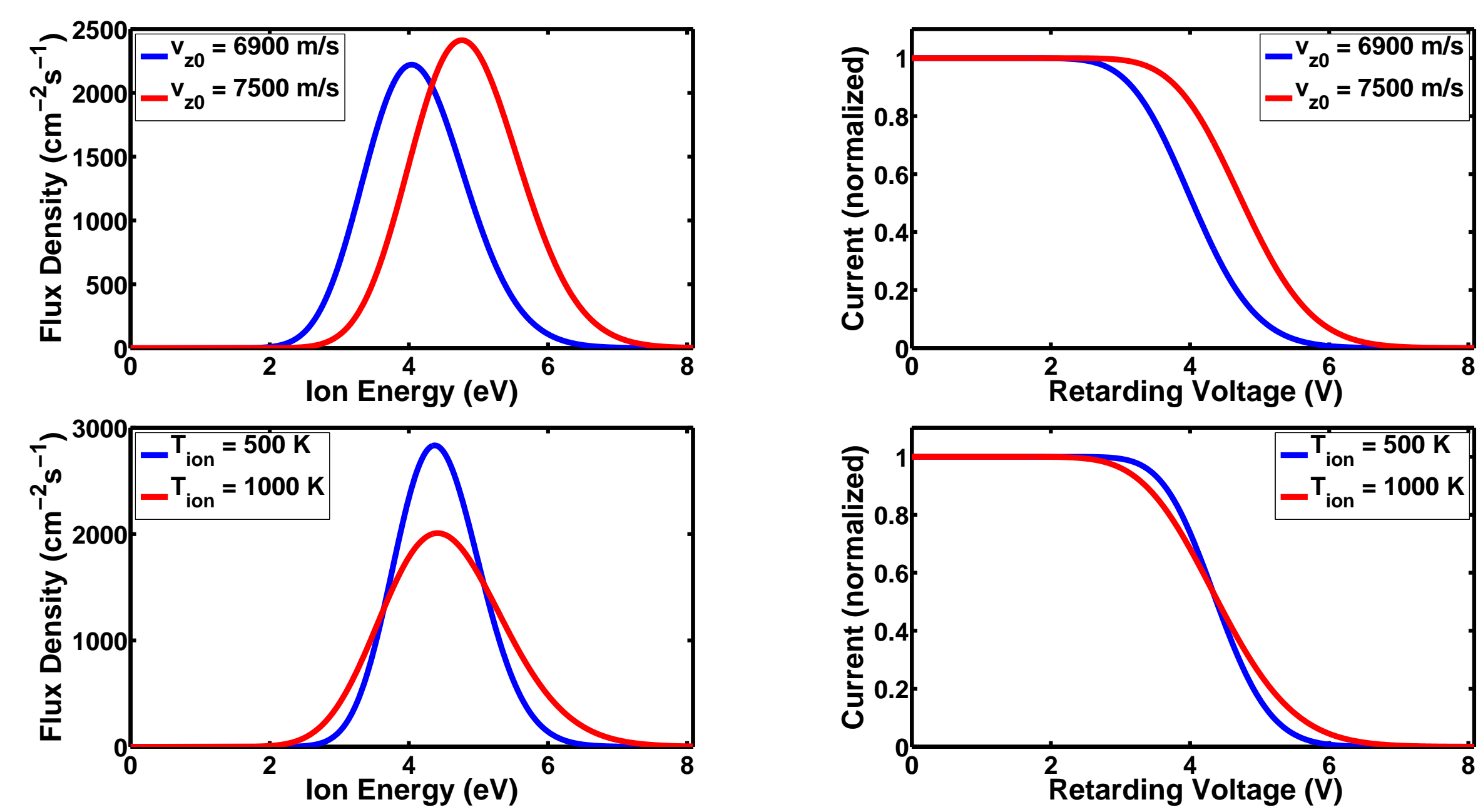


Figure 1: The relation of IV curves collected by an ideal RPA to the corresponding flux density distributions for  $O^+$  ions. The IV curve is the integral of the flux distribution above a specified value as described in Equation 1. The top row shows variation with ram velocity. The inflection point in the IV curve is related to the mean ram velocity of the distribution. Higher velocities will be centered about higher energies. The bottom row shows variation with ion temperature. A colder distribution will have a more narrow spread in energy space, which results in a steeper slope in the IV curve. Note that the inflection point is unchanged for these two IV curves.

The current through an aperture area  $A$  of a typical RPA (which is laid perpendicularly to the  $z$ -axis and is at rest with respect to the ions) is described by

$$I(\phi_{RV}) = q_0 A N_0 \int_{v_{z0}} \int_{v_{z0}} \chi(\vec{v}, \phi_{RV}) v_z D(\vec{v}) d\vec{v}. \quad (1)$$

where  $N_0$  is the total density of particles,  $D(\vec{v})$  is the velocity distribution of particles outside the instrument,  $v_z$  is the particle speed toward the aperture,  $\vec{v}$  is the 3D vector particle velocity, and  $q_0$  is the fundamental charge. The transmission of ions with initial velocity  $\vec{v}$  through the grid stack for applied retarding potential  $\phi_{RV}$  is defined as  $\chi(\vec{v}, \phi_{RV})$ . Ideally, the transmission is described by a step function, where all ions below the stopping velocity ( $v_z = \sqrt{2q_0\phi_{RV}/m}$ ) are rejected. There is no alteration in transmission based on cross-track velocity of the individual ions. If the distribution is considered to be a drifting Maxwellian, Equation 1 reduces to the form used by Whipple (1959), which integrates to the simple analytic form

$$I(\phi_{RV}) = \frac{q_0 A \chi_0 N_0 v_{z0}}{2} \left[ 1 + \text{erf}(\kappa) + \frac{v_h}{v_{z0}\sqrt{\pi}} e^{-\kappa^2} \right] \quad (2)$$

where  $\kappa = (v_{z0} - \sqrt{2q_0\phi_{RV}/m})/v_h$  and  $\phi_{RV}$  is the stopping potential. This equation is typically used in conjunction with a non-linear least-squares routine (Marquardt, 1963) to extract temperatures and velocities from IV curves.

## Problems with the Ideal Assumptions

Many of the assumptions discussed above do not hold for real grids, and it is the purpose of this poster to investigate the departures from Equation 2 that exist in practice. For example, Hanson *et al.* (1972) shows that for any real grid geometry, the potential in the plane of the grid is non-uniform, allowing some ions with energies less than the stopping energy to leak through the filter. This creates a transmission dependence based on particle trajectory relative to the individual wires that comprise the grid, in addition to particle energy and angle. The amount of leakage will be determined by the instrument geometry and the potentials applied throughout. Additionally, ions having energies slightly greater than the stopping energy ( $q_0\phi_{RV}$ ) may be translated around the grid wire, increasing the transmission for these particular energies to a value greater than the optical transparency. Both of these effects are largest for particle energies near the stopping potential, and both will increase the total current collected for a given applied bias. The instrument also has a limited acceptance cone defined by the geometry and the relative velocities of the spacecraft and particles, which tends to reduce the current. All of these effects alter  $\chi(\vec{v}, \phi_{RV})$  from the idealized step-function expression, resulting in a measured current which relates to the distribution function differently than expected from Equation 2. In order to understand the complicated relation between the distribution function and the measured data, the transmission function incorporating all of these non-ideal effects must be investigated in detail.

## Numerical Model

The numerical model consists of a slice out of an instrument with infinite dimensions in the  $xy$ -plane, as shown in Figure 2a. Because the geometric features of a grid are periodic in both dimensions of the grid plane, the model section is taken along the grid wires and reflective boundaries are set over  $x$  and  $y$  to simulate stretching the grid planes out to infinity. This approach does not explicitly consider edge effects at the grid boundaries, but these can be minimized by proper geometric device design. Because the greatest perturbations to the trajectories occur at grid potentials near the ion energies of interest, the effects of grids held at ground or negative voltages are neglected. (At the altitudes where RPAs are used in near Earth, all ions are positively charged.) The grids in the energy filter are modeled as real flat (*i.e.*, not woven) grids, while other grids are modeled as ideal planes. As in flight instruments, the grids are equally spaced and the first grid in the energy filter has twice the linear wire density of the second grid. The aperture grid (and a small buffer region outside the instrument model) is grounded. This grid is labeled G1 in Figure 2b. The retarding grids (G2) are swept from 0.0 – 8.5 V. The suppression grid (G3) has a large negative potential to prevent electrons from contributing to the current. A shield grid (not shown) lies beyond the suppression grid and has a small negative potential to prevent secondary electron emission from the collector. This study neglects the shield grid since it does not significantly alter the ion collection statistics.

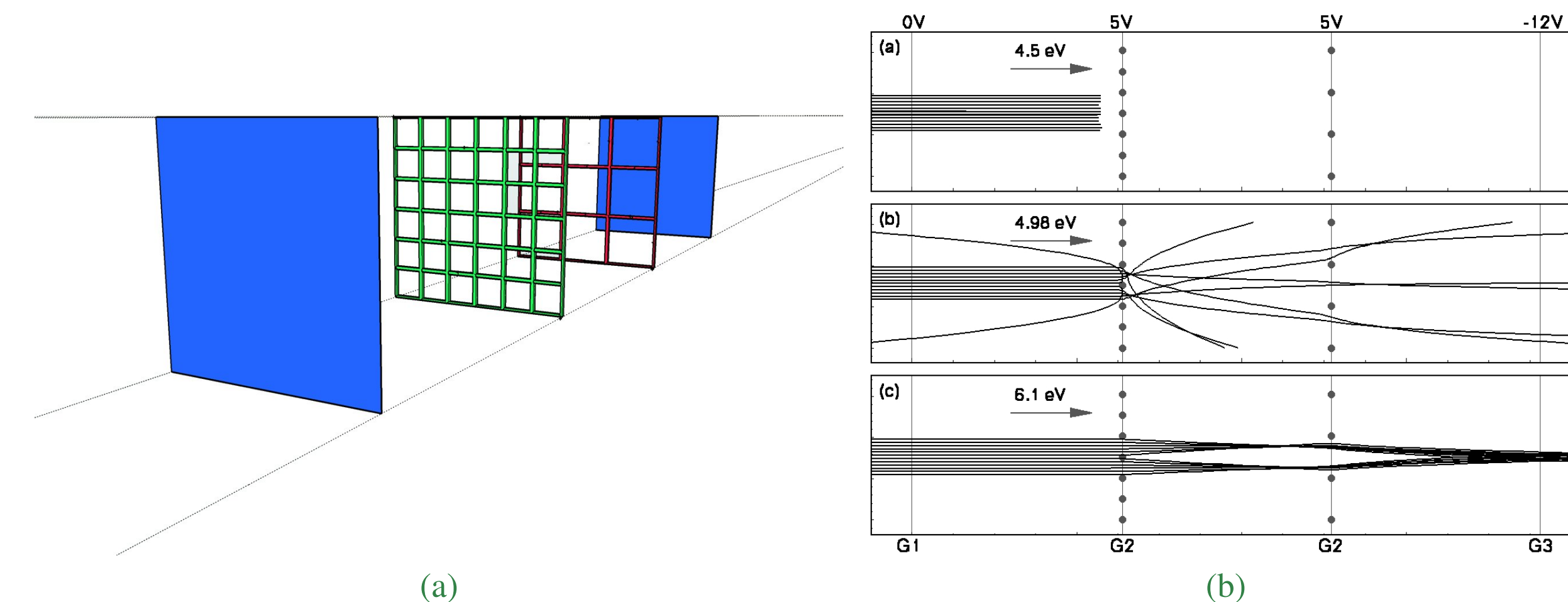


Figure 2: The model built in ANSYS shown in three dimensions (a) and ion tracks through a two-dimensional slice (b). The sample ion tracks through the 2D model show three different effects.

The three subplots in Figure 2b show the effects of the non-uniform potential on ion trajectories over a two-dimensional slice of the numerical model. Three clear effects are seen:

- Ions of sufficiently low energies are repelled by the first retarding grid. None are collected.
- A small fraction of ions just below the stopping energy leak through the retarding grid. Those near the center of each grid cell will slip through, and those near the wires are repelled. This always results in an increase in expected current above the ideal.
- Ions with energies greater than the stopping value undergo a process analogous to optical lensing. The spatial distribution of ions beyond the first retarding grid is drastically altered from the initial uniform distribution. The position of the second retarding grid with respect to the first grid is important in determining the transmission of ions to the collector.

Because the relative alignment of the two retarding grids is essential to calculating the transmission of ions through the grids, two bounding models are chosen. Model A is described as being ‘perfectly aligned,’ such that the focal point of each ion lens does not pass through a wire in the second grid. Model B is described as being ‘perfectly misaligned,’ where three out of four focal points pass through wires from the second grid. A more detailed description of the effects of grid alignment on transmission statistics can be found in Klenzing *et al.* (2008).

## Transmission of Ions

The transmission effects described in the previous chapter are not observed individually, but as a cumulative effect across the entire distribution, as observed in Figure 3. The velocity distribution of  $O^+$  ions external to the RPA is the same in all cases- a one-dimensional Maxwellian distribution centered at a velocity of 7200 m/s and with a thermal spread of 750 K. The distribution is plotted as ion flux density vs ion energy. The shaded portion of each curve is the flux transmitted through the retarding grids with an applied retarding potential of 4 V. (Note that this is for a distribution with no thermal variation in the cross-track dimensions.) The measured current will be related to the integral of the curve, or the shaded area. The black area in panel (a) is the portion transmitted in an ideal case (nothing below the cutoff value, and a constant fraction of ions above this cutoff value are transmitted). The colored areas in panels (b)-(d) were calculated by the real transmission values from the ANSYS simulations for ions moving normal to the grid plane.

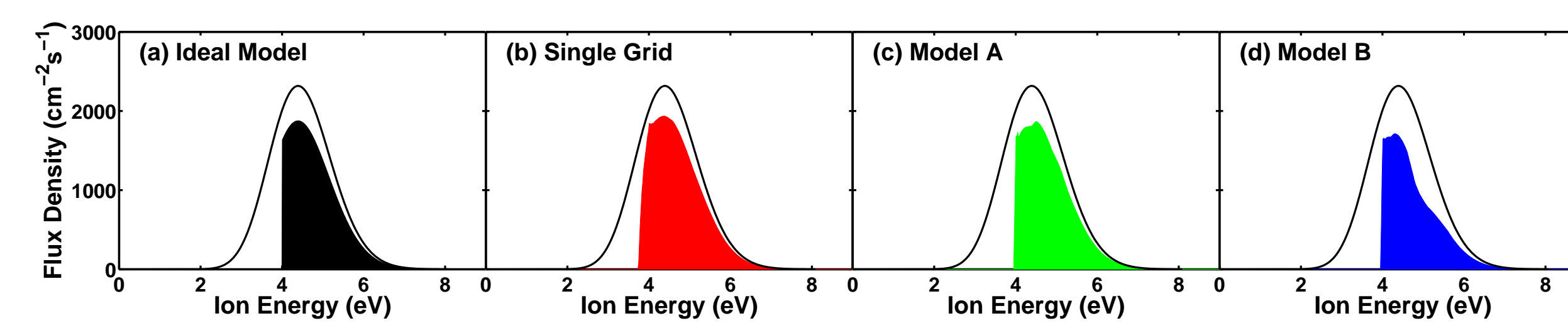


Figure 3: The effect of three different grid models on the transmission of a one-dimensional Maxwellian distribution of  $O^+$  ions with velocities normal to the grid plane. The retarding potential is at 4 V in all cases. The distribution is centered about 7200 m/s and has a thermal spread of 750 K. The measured current will be the shaded portion of each curve. Panel (a) shows ideal transmission in black. The shaded region in panel (b) shows the transmitted ion flux for a single grid system. Panels (c) and (d) show the transmitted distributions for real grid Models A and B, respectively.

The curve from the single grid model is shown in red in Figure 3b. The area is substantially increased over that from the ideal case (Figure 3a), particularly in the area below 4 eV. This region is the portion of the current due leakage of ions through the non-uniform potential in the plane of the grid. The curves from Model A and B (panels (c) and (d)) reveal much about the effect of double-grid systems on measured current. The leakage effects are indicated by the transmission of ions below 4 eV in both graphs, and the lensing effects are noted by the curvature of the region above 4 eV. It is inferred from these graphs that the change in current due to the lensing effects is much greater than the change due to the leakage effects, at least for normal incidence. The leakage effects are dramatically reduced from the single grid case.

## Inherent Deviations in Inferred Parameters

A case study was completed using the Monte Carlo simulation for a Maxwellian distribution with a three-dimensional thermal spread of  $O^+$ . For each grid model, 5000 sets of simulated IV curves were generated, each with a set of input parameters randomly generated for ram velocities between 6900 and 7500 m/s and temperatures between 500 and 1000 K. Although in the upper atmosphere temperature may be as high as 5000 K, this smaller range of temperatures was chosen to ensure that the bulk of  $O^+$  ions would fall into a narrow cone of attack angles. A set of IV curves was generated for the ideal Whipple Equation (see Equation 2) and the three non-ideal models. Each curve consists of a 17 point IV curve, using the same spacing of voltages as on the C/NOFS RPA. A cone of acceptance of  $\eta = 45^\circ$  was used for the simulations discussed here, though no significant difference was detected in simulations run with a cone of acceptance of  $\eta = 90^\circ$ . The IV curves were generated using the mean-sample method of integration for Equation 1 (Rubinstein, 1981).

Figure 4 shows the cumulative errors for the fits to the IV curves generated by each model. The errors are plotted as two-dimensional histograms of each error (fit value minus input value) versus the input values of ram velocity and ion temperature. The ideal expression (Equation 2) is plotted in the first row to establish the baseline error in the fitting routine. These errors are attributed to the spacing of voltages for which the IV curves are calculated.

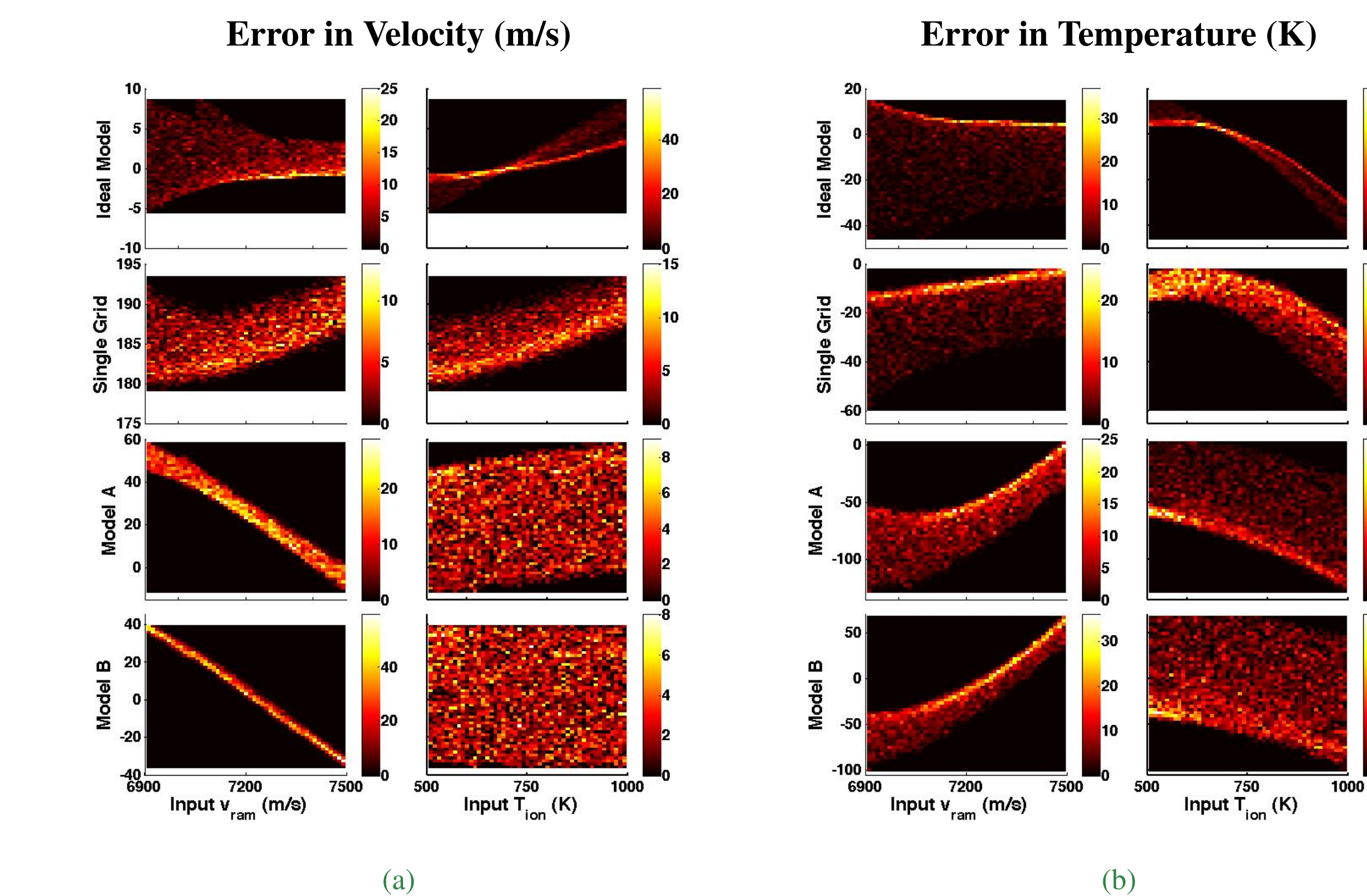


Figure 4: Errors in the inferred parameters from the four numerical models. The histograms show the frequency of occurrence for error in a fitted parameter versus the input parameter. The eight plots in column (a) show the errors in ram velocity. The eight plots in column (b) show the errors in ion temperature. The error is defined as the difference between the fitted value and the input value. All simulated IV curves were for Maxwellian distributions with a three-dimensional thermal spread and a three-dimensional net drift with respect to the instrument. Correlation of error to cross-track drift is not plotted as there is no significant correlation found.

It is readily seen that the magnitude of error is strongly affected by the model used. The following can be inferred from the above plots:

- The magnitude of all errors increase with input temperature for all models. Because this effect is seen in the ideal simulation as well, this is attributed to the spacing of voltages used. Improvements in performance would likely result from additional carefully chosen RV values.
- The double-grid models have a much lower average error in velocity than the single grid model. This is attributed to a more uniform potential in the plane of the first retarding grid for the double-grid setup and confirms the results predicted analytically by Hanson *et al.* (1972).
- The double-grid models have a larger average error in temperature than the single grid model. This is attributed to the lensing effects dominant in the double-grid models.
- The errors in velocity for all double-grid models are strongly anti-correlated to the input velocity. Additionally, there is a correlation between temperature error and input velocity. This allows a fairly straightforward method of computing correction factors for spacecraft data.

Table: The average errors and standard deviations for the four simulation models.

	Ideal Model	Single Grid	Model A	Model B
Ram Velocity	$0.9 \pm 2.5 \text{ m/s}$	$185.8 \pm 2.9 \text{ m/s}$	$24.3 \pm 17.7 \text{ m/s}$	$-2.4 \pm 21.5 \text{ m/s}$
Ion Temperature	$-8.0 \pm 13.8 \text{ K}$	$-16.8 \pm 10.6 \text{ K}$	$-62.0 \pm 27.9 \text{ K}$	$-15.0 \pm 38.3 \text{ K}$

This method of simulation was run multiple times to investigate the effects of a net cross-track drift of ions on the magnitude of the errors. The three final studies used for each model were:

- No net cross-track drift in any of the 5000 IV curves.
- A constant net drift of 500 m/s was added to the drift of each of the 5000 IV curves.
- The input net cross-track velocities were allowed to vary in both planar dimensions such that the maximum value of  $\sqrt{v_{z0}^2 + v_{y0}^2}$  would be 500 m/s.

There was no significant change in the histogram plots of error for any of these three variations. The plots above are from the third case (where cross-track velocity is allowed to vary). This shows that despite the perturbations of the ion trajectories by the grids, the RPA measurements are not influenced in any statistically significant way by cross-track drift.

## Discussion

The results shown in this poster are significant for the interpretation of RPA data. Assuming that the effects from grids dominate, a simple method for constructing first-order corrections to satellite data has been developed to demonstrate this. Because of the limitations of the simulation method, this correction technique is valid only for cold distributions of  $O^+$ . A subset of data from the C/NOFS RPA that fit into this narrow window was chosen for this demonstration, as seen in Figure 5. For each fitted velocity/temperature pair from the satellite data, the closest matching fit values from both the Model A and Model B simulations were chosen as a match. The corresponding error value was subtracted from the satellite fit value to provide the correction. To determine which simulation set most closely matched the satellite fit pair, the temperatures were converted to a thermal velocity and the distance in velocity space between the two values was computed. The smallest distance was chosen as the best match, and any distance greater than 5 m/s was eliminated from consideration.

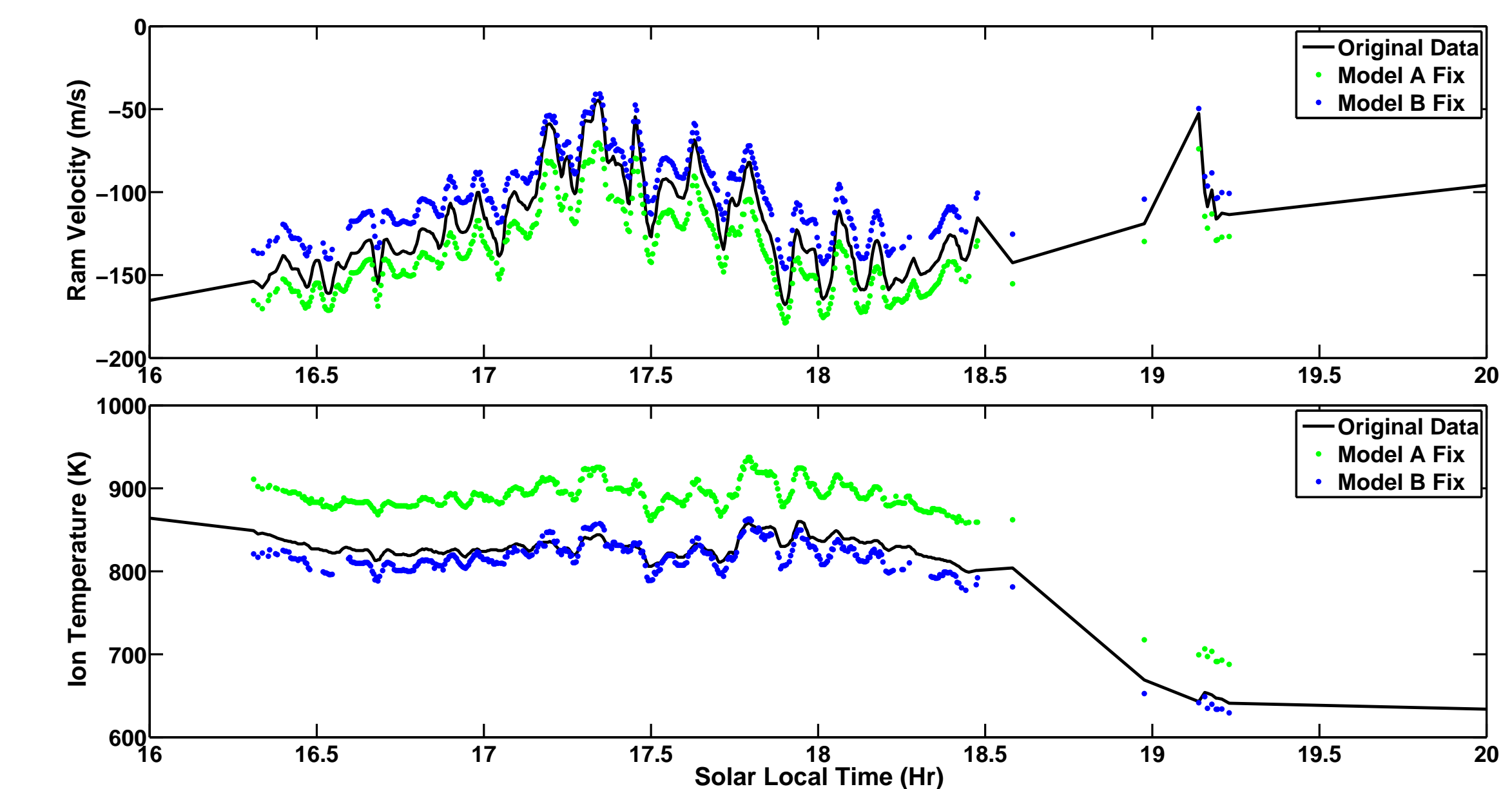


Figure 5: A sample plot of satellite data taken from the C/NOFS RPA. The solid line represents the original parameters as fit by a least squares method. The colored dots are corrections applied based on the results of the simulation, assuming that the effects of the grids are dominant source of error. The performance of the flight instrument is expected to be somewhere between Models A and B. The original data is for 99%  $O^+$  or greater.

The two models were chosen as bounding cases for the infinite variety of grid alignments that are possible in flight instruments. Thus these ‘fixed’ values should be interpreted as establishing a region of confidence around the fitted values.

## Conclusions

- There is a significant improvement in velocity accuracy from a double grid RPA over that from a single grid system.
- The errors in temperature increase in the double grid system over that from the single grid system.
- There is a strong correlation of both velocity and temperature errors to input ram velocity.
- There is no significant correlation to cross-track drift.
- Results indicate that a computational analysis technique to infer physical parameters from RPA data may significantly improve the quality of geophysical data.

## Future Work

There are many tasks still to be done to better understand the inherent uncertainty in RPA data. A multi-species version of the simulation must be developed if corrections are to be applied to old data. The simulation can also be used to determine future changes to instrumentation to improve the accuracy of the inferred parameters. An empirical study designed to complement the simulation work here is currently in progress.

## References

- Hanson, W.B., D.R. Frame, J.E. Migdely, *J. Geophys. Res.*, **77**, 1914-1922, 1972
- Klenzing, J. H., G. D. Earle, and R. A. Heelis, *Phys. Plasma*, **15**, Art. no. 062905, 2008
- Marquardt, D. W., *J. Soc. Ind. and App. Math.*, **11**, p. 431, 1963
- Rubinstein, R. Y., *Simulation and the Monte Carlo Method*, John Wiley and Sons, 1981
- Whipple, E.C., *Proc. of the Inst. of Rad. Eng.*, **47**, (11), 2023-2024, 1959

## Acknowledgments

This work was supported by NASA grant NNG05-GL70H. The authors would like to thank Dr. Robert Pfaff for sponsoring this project for NASA. This poster was typeset in L<sup>A</sup>T<sub>E</sub>X.

## For More Information

Please contact jeffk@utdallas.edu. This poster is available online at [www.utdallas.edu/~jeffk](http://www.utdallas.edu/~jeffk)